"Hairy" Plates: Poly(ethylene oxide)-*b*-polyisoprene Copolymers in the Presence of Laponite Clay

D. Gournis† and G. Floudas*,‡

Department of Materials Science and Engineering, and Department of Physics, University of Ioannina, P.O. Box 1186, 451 10 Ioannina, Greece

Received December 3, 2003. Revised Manuscript Received February 4, 2004

The morphology and thermal properties have been investigated in laponite/poly(ethylene oxide) (PEO) clay/homopolymer and laponite/poly(ethylene oxide-*b*-isoprene) (PEO−PI) clay/block copolymer nanocomposites using small- and wide-angle X-ray scattering, optical microscopy, transmission electron microscopy, and differential scanning calorimetry. In the laponite/PEO composite, PEO intercalation adjusts the layer spacing and increases the layer correlation length. In the laponite/PEO−PI nanocomposite, the enthalpic interactions between the unlike blocks favoring nanophase separation work in tandem with the entropic interactions favoring polymer/clay intercalation, giving rise to multiple levels of organization. We show that (i) a diblock copolymer can be effectively intercalated within the clay galleries and (ii) the balance of these interactions give rise to a case where one block of the copolymer is intercalated and the other forms a spring that keeps the clay platelets apart, i.e., "hairy" plates.

Introduction

Polymer−clay nanocomposites are divergent organic−mineral composites that can be successfully integrated, forming new "hybrid" materials.[1,2] The first practical application of a nanocomposite was the nylon−montmorillonite clay system that displayed a large increase in tensile strength, modulus, and heat distortion temperature without loss of impact resistance.[3,4] Since then, the field has rapidly expanded using different polymer/clay systems, giving rise either to exfoliated or to intercalated systems. Typical preparation methods of these nanocomposites include solution intercalation, melt intercalation, and in-situ polymerization. Solution intercalation, in particular, has been very successful in incorporating delaminated clay into polymers.[1] Examples include water-soluble polymers, such as poly(ethylene oxide) (PEO). Solution intercalation is thought to be an entropy-driven process, where the translational entropy gained by desorption of solvent molecules from the clay interlayer compensates for the entropy decrease of the confined polymer chains.

Nanocomposites based on PEO intercalated between the layers of mica-type silicates represent a new class of polymer composite electrolytes with possible applications as solid-state lithium batteries.[5−8] In particular, PEO intercalated between 0.96-nm-thick, negatively charged montmorillonite layers have been studied.[9−11] Recent experiments[10] and computer simulations[9,11] on PEO/montmorillonite nanocomposites suggested that the PEO chain conformation within the clay is not of the usual all-trans or helical conformation but forms a layered yet disordered structure.

In the present study, we investigate the morphology in laponite[12−14] (a synthetic hectoride)/PEO and for the first time in laponite/poly(ethylene oxide-*b*-isoprene) (PEO−PI) clay/block copolymer nanocomposites. In the former system, we find that PEO intercalation adjusts the layer spacing and increases the layer correlation length. The latter system combines the entropic interactions, favoring polymer/clay interactions with the strong enthalpic interactions between the two unlike blocks of the copolymer favoring nanophase separation.[15] We show that this delicate balance of interactions is the key in designing some new structures, such as the "hairy" plates, where one block of the copolymer is intercalated in the clay galleries and the other forms a spring that keeps the clay platelets apart. We employ small- and wide-angle X-ray scattering, optical microscopy, and transmission electron microscopy for the structure investigation and differential scanning calorimetry for the thermal properties.

* To whom correspondence should be addressed.
† Department of Materials Science and Engineering.
‡ Department of Physics.

(1) *Polymer-Clay Nanocomposites*; Pinnavaia, T. J., Beall, G. W., Eds.; J. Wiley & Sons: New York, 2001.
(2) Jacob, M. M. E.; Hackett, E.; Giannelis, E. P. *J. Mater. Chem.* **2003**, *13*, 1.
(3) Kojima, Y.; Usuki, A.; Kawasumi, M.; Okada, A.; Kurauchi, T.; Kamigaito, O. *J. Polym. Sci., Polym. Chem.* **1993**, *31*, 983.
(4) Ioannou, E.; Floudas, G.; Giannelis, E. P. In preparation.
(5) Gadjourova, Z.; Andreev, Y. G.; Tunstall, D. P.; Bruce, P. G. *Nature* **2001**, *412*, 520.
(6) Zhao, Q.; Samulski, E. T. *Macromolecules* **2003**, *36*, 6967.
(7) Doeff, M. M.; Reed, J. S. *Solid State Ionics* **1998**, *113*, 109.
(8) Sandi, G.; Joachin, H.; Kizilel, R.; Seifert, S.; Carrado, K. A. *Chem. Mater.* **2003**, *15*, 838.
(9) Hackett, E.; Manias, E.; Giannelis, E. P. *Chem. Mater.* **2000**, *12*, 2161.
(10) Strawhecker, K. E.; Manias, E. *Chem. Mater.* **2003**, *15*, 844.
(11) Kuppa, V.; Manias, E. *Chem. Mater.* **2002**, *14*, 2171.
(12) Balnois, E.; Durand-Vidal, S.; Levitz, P. *Langmuir* **2003**, *19*, 6633.
(13) Labbe, P.; Reverdy, G. *Langmuir* **1988**, *4*, 419.
(14) Pignon, F.; Magnin, A.; Piau, J.-M.; Cabane, B.; Lindner, P.; Diat, O. *Phys. Rev. E* **1997**, *56*, 3281.
(15) Hadjichristidis, N.; Pispas, S.; Floudas, G. In *Block Copolymers: Synthetic Strategies, Physical Properties and Applications*; J. Wiley & Sons: New York, 2002.

10.1021/cm035267m CCC: $27.50
Published on Web 03/25/2004

Table 1. Molecular Characteristics of the Diblock Copolymers and PEO Homopolymer

sample	M_n PEO	M_n PI	M_n total	M_w/M_n	wt % PI	f_{PEO}	phase state
PEO−PI 20−11	19 700	10 600	30 300	1.12	0.35	0.596	$L_c \xrightarrow{344}$ Lam
PEO−PI 21−5	21 000	5 400	26 400	1.11	0.205	0.75	$L_c \xrightarrow{325}$ Hex
PEO	20 000			1.05			
PE	20 000			1.05			

Experimental Section

Samples. The clay used in this work was laponite RD, a synthetic trioctahedral hectorite composed of two tetrahedral silica sheets and a central octahedral magnesia sheet, obtained from Laporte Industries Ltd.[12−14] The particles have a negative charge that is balanced by Na^+ counterions located around the clay platelets. The structural formula for laponite, as determined from chemical analysis, is

$Na_{0.8}[Mg_{5.4}Li_{0.4}]Si_8O_{20}(OH)_4$,

and its cation exchange capacity (CEC) measured by the Co(II) procedure is 48.1 mequiv/100 g of clay. Sodium-exchanged samples were prepared by immersing the clay into a 1 N solution of sodium chloride. Cation exchange was completed by washing and centrifuging four times with dilute solution of NaCl. The samples were finally washed with distilled−deionized water, transferred into dialysis tubes in order to obtain chloride free clays, and then dried at room temperature. Two PEO−PI diblock copolymers have been used in the present study.[16] The molecular characteristics are given in Table 1 and details on the synthesis can be found elsewhere.[16,17] The melt phase state for the two diblocks differs; the PEO−PI 20−11 forms a lamellar mesophase, whereas the PEO−PI 21−5 forms a hexagonal mesophase composed of PI cylinders in a PEO matrix. Upon cooling, these equilibrium morphologies revert to the crystalline lamellar due to the onset of PEO crystallization. The complete phase diagram of the PEO−PI diblock copolymer system has recently been reported.[16] In addition, PEO and polyethylene (PE) homopolymers were used, and their molecular characteristics are also included in Table 1. Films of polymer−clay nanocomposites were prepared as follows: 50 mg of PEO or diblock copolymer diluted in 0.6 mL of H_2O was added to 0.6 mL of aqueous clay suspensions in different polymer-to-clay ratios R of 10, 5, ..., 0.5 (where, R = [mass of PEO]/[mass of clay]). The mixtures were stirred for 3 h and then air-dried by spreading on glass plates. For PE, the following procedure was used: the polymer and clay were dissolved in toluene and acetonitrile, respectively, and their mixtures were stirred and dried on glass plates.

Polarizing Optical Microscopy (POM). A Zeiss polarizing optical microscope was used together with a Linkam heating stage (THMS 600) with a temperature programmer. Two experiments were made: first, by slow cooling from 473 to 303 K and second by heating to an initial temperature (T = 373 K), i.e., above the PEO melting point, and by performing isothermal crystallization experiments at different final temperatures in the range from 323 to 333 K. In both experiments, images were recorded with a CCD camera. In the case of PEO homopolymer, the usual spherulitic superstructure was observed, and the corresponding (linear) growth rates (G) are plotted in Figure 1 as a function of crystallization temperature (T_c).

In the same figure the (linear) growth rates from the laponite/PEO−PI 21−5 composite, with a weight fraction of w_{PEO-PI} = 0.91, are plotted as a function of crystallization temperature. Spherulites are again observed, but their shape is truncated (inset to Figure 1) and their growth rate has decreased by 3−4 orders of magnitude relative to the PEO homopolymer. This is a composite effect; the PEO growth rates in the PEO−PI diblock copolymers are already slower than the PEO homopolymer, but the addition of the clay particles decreased further the growth rate. The observed spherulitic superstructure in the clay/copolymer nanocomposites with low clay content suggests crystallization within the continuous PEO phase (PEO forms the matrix in the PEO−PI 21−5 copolymer) and three-dimensional growth. In the laponite/PEO−PI 20−11 nanocomposite with w_{PEO-PI} = 0.91, no spherulites but rather a featureless birefringence was observed. Strongly birefringent objects (nonspherulitic) are also obtained for the composites with the higher clay content.

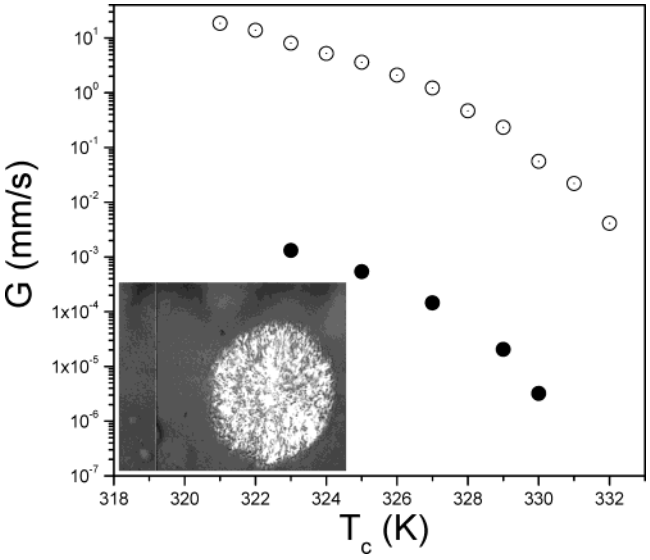

Figure 1. Spherulitic growth rates from a PEO homopolymer (open symbols) and the laponite/PEO−PI 21−5 with w_{PEO-PI} = 0.91 nanocomposite (filled symbols) as a function of crystallization temperature, following a temperature jump from 353 K. Truncated spherulites are observed in the nanocomposite case (inset).

X-ray Scattering. Both wide-angle and small-angle X-ray scattering (WAXS and SAXS) measurements have been performed for the PEO homopolymer, the different diblock copolymers, and the clay/polymer nanocomposites. For the WAXS measurements the X-ray powder diffraction data were collected on a D8 Advance Bruker diffractometer by using Cu Kα (40 kV, 40 mA) radiation and a secondary beam graphite monochromator. The patterns were recorded in the 2θ range from 2° to 80°, in steps of 0.02°, and the counting time was 2 s per step. In addition, temperature-dependent measurements were made with a Siemens θ-θ diffractometer (model D500T) in the reflection geometry. A Cu Kα radiation was again used from a Siemens generator (Kristalloflex 710 H) operating at 35 kV and 30 mA, and a graphite monochromator was utilized in front of the detector (λ = 0.154 nm). Measurements were made in the 2θ range from 0.1° to 40° in steps of 0.01° within the temperature range from 303 to 503 K. SAXS measurements were performed using an 18 kW rotating anode X-ray source with a pinhole collimation and a two-dimensional detector (Siemens) with 1024 × 1024 pixels. The sample-to-detector distance was 1.46 m. One hour long measurements

(16) Floudas, G.; Vazaiou, B.; Schipper, F.; Ulrich, R.; Wiesner, U.; Iatrou, H.; Hadjichristidis, N. *Macromolecules* **2001**, *34*, 2947.
(17) Floudas, G.; Ulrich, R.; Wiesner, U. *J. Chem. Phys.* **1999**, *110*, 652.

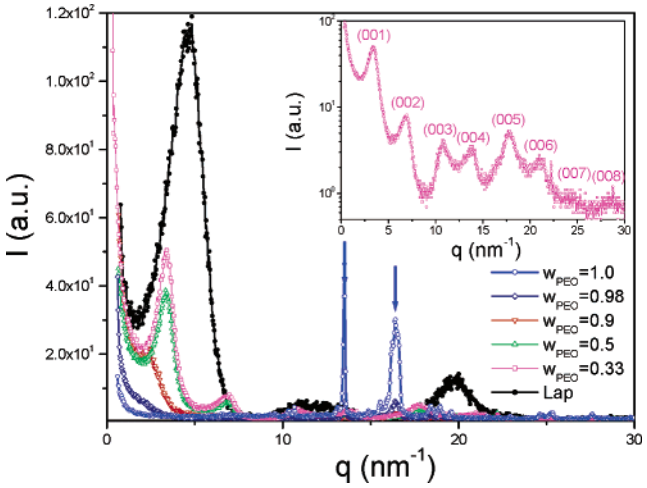

Figure 2. Wide-angle X-ray scattering patterns from the pure laponite (filled circles), the PEO homopolymer, and the laponite/PEO nanocomposites with PEO weight fractions 0.33, 0.5, 0.9, and 0.98 at 303 K. Arrows give the intense reflections corresponding to the PEO unit cell. Notice the broad diffraction peaks of the pure laponite and the improved correlations in the nanocomposites. In the inset, the diffraction pattern of the laponite/PEO with a 33% weight fraction of PEO is shown for clarity and exhibits a more regular structure (higher order reflection up to the eighth order). The polymer elasticity improves the lateral order of laponites.

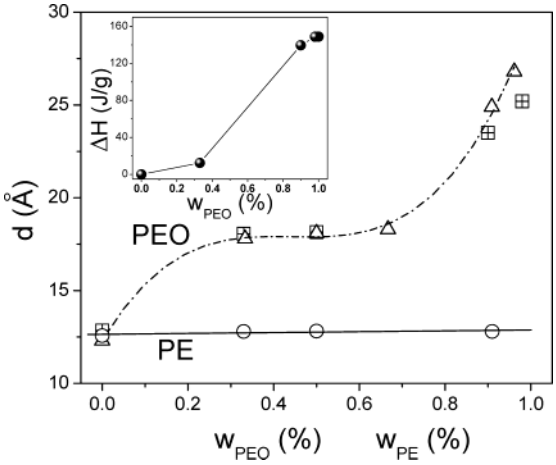

Figure 3. Dependence of the primary WAXS reflection in clay/PEO nanocomposites as a function of polymer fraction. Two different clays have been used: laponite (open triangles) and sodium montmorillonite (open squares). The case of laponite/PE is also shown for comparison. In the inset, the heat of fusion is shown associated with the melting of PEO in the laponite/PEO nanocomposites as a function of the polymer content obtained from DSC.

were made while cooling the sample at different temperatures from 353 K (i.e., above the melting point of PEO) to 303 K.

Transmission Electron Microscopy (TEM). A LEO EM 912 transmission electron microscope with integrated electron energy-loss spectrometer, operated at 120 kV, was used. Dilute aqueous solutions of laponite/PEO−PI copolymer nanocomposites were deposited on metal grids, and the solvent was allowed to evaporate slowly at ambient temperature. TEM images were taken both before staining and following staining with OsO_4 vapor. Micrographs were recorded on Ilford PAN F 35 mm film.

Differential Scanning Calorimetry (DSC). A Mettler Toledo Star DSC capable of programmed cyclic temperature runs over the range 113−673 K was used. Samples were first heated with a rate of 10 K/min to 373 K and subsequently cooled to 153 K. A second heating/cooling cycle was performed with the same heating/cooling rate and the (apparent) melting and glass transition temperatures were obtained from the second heating run.

Results and Discussion

The diffraction patterns of the laponite/PEO nanocomposites, shown in Figure 2, display several features that are worth noticing. The pure laponite exhibits intense, albeit broad, diffraction peaks suggesting irregular stacking of layers with an average spacing of 1.25 nm. Notice that this spacing is larger than the d_{001} spacing of dry laponite (0.96 nm), and the difference is attributed to the presence of a single layer of hydrated Na^+ exchangeable cations.[13] For the PEO homopolymer, the sharp diffraction peaks reflect the monoclinic unit cell with a unit cell parameter of 0.193 nm along the helical axis.[18] In the nanocomposites, the primary reflection shifts to lower scattering vectors q, and in addition, higher order reflections appear, suggesting improved layered stacking in the presence of PEO. This is better shown in the inset to Figure 2, where diffraction peaks up to eighth order are shown for the laponite/PEO with w_{PEO}=0.33. Employing the Debey−Scherrer equation $Nd = K\lambda/\beta \cos\theta$ [where N is the number of diffraction layers along the c-axis, d is the 001 spacing of one layer (in Å), K is a constant near unity ($K = 0.91$), λ is the wavelength of X-rays ($\lambda = 1.5418$ Å), θ is the angular position of the first diffraction peak, and β is the broadening of the 001 diffraction line (calculated at full width at half the peak height and expressed in radians], the average stacking height of the layers can be estimated. We obtain that the average stacking height in the laponite/PEO system is doubled relative to the pure laponite ($N = 2$ vs $N = 4$ in the laponite and composite, respectively). Clearly, the elasticity provided by the PEO chains plays an important role in adjusting the layer spacing, improving therefore the layer correlation length. In all cases it is observed that PEO crystallizes (see below) in the presence of clay and the nucleation sites are likely to be located away from the clay particles.[10]

The corresponding d spacings for the laponite/PEO system are plotted in Figure 3. For a range of intermediate polymer concentrations the d spacing is about 1.8 nm.

The increase in the interlayer distance from 1.25 to 1.8 nm is compatible with the following two possible PEO conformations: (i) a bilayer of chains in a planar zigzag conformation[9] or (ii) a single layer of intercalated PEO chains adopting a helical conformation. The latter implies intracrystalline type of arrangements of the PEO chains as opposed to a more liquidlike structure. For higher polymer concentrations, the characteristic spacing increases further to about 2.6 nm, corresponding to an increased number of PEO layers making the layer-by-layer scenario more plausible. To explore the generality of this picture for the intercalated PEO chains, we have prepared composites of PEO with a natural sodium montmorillonite (MMT), SWy-1, obtained from the Source Clay Minerals Repository at the University of Missuri, following the same preparation protocol at similar compositions. The resulted d spacing is included

(18) Floudas, G.; Tsitsilianis, C. *Macromolecules* **1997**, *30*, 4381.

also in Figure 3. The two sets of data are in excellent agreement (also with published data for the MMT/PEO system[10]), suggesting the picture of layer-by-layer PEO intercalation in clays. Contrast this with the laponite/PE mixtures, where intercalation is not possible when prepared by solution intercalation. A different preparation method based on the polymerization-filling technique has been reported to result in PE intercalation.[19] Notice that in all cases PEO crystallizes, as shown by the exothermal peaks in the DSC, and the heat of fusion (ΔH) upon crystallization is shown in the inset to Figure 3. The degree of crystallinity of pure PEO is 75% ($X_c = \Delta H/\Delta H_0$, where ΔH_0 refers to the heat of fusion of a 100% crystalline PEO) and reduces to 7% when $w_{PEO} = 0.33$.

Next we examine the structure in the PEO−PI diblock copolymers in the presence of laponite clay. The block copolymer comprises a hydrophilic (PEO) and a hydrophobic (PI) block and only the hydrophilic block can intercalate into the clay (attempts on PI/clay solutions to intercalate the PI chains failed). Thus, one block has the tendency to intercalate but the other block avoids intercalation. In that respect, the clay particles act as barriers for the PI block and can effectively increase the tendency for block segregation. On the other hand, the unfavorable interactions of the PI block with the clay could also lead to a phase separation (macrophase separation) of the clay and of the diblock copolymer. To explore these possibilities, we have investigated the thermal and structural properties of the composites using DSC and WAXS, SAXS, TEM, respectively.

The thermal properties of the laponite/diblock copolymer system are distinctly different from those of the laponite/PEO system. Figure 4 compares the DSC traces of two composites based on laponite/PEO−PI 20−11 with different diblock content ($w_{EI} = 0.5$ and 0.91). The crystallization/melting temperatures are observed during the cooling/heating cycle of the laponite/PEO−PI 20−11 with $w_{EI} = 0.91$ and the associated heat of fusion is 88 J/g, suggesting a degree of crystallinity (X_c) of 48% for the PEO block. At lower temperatures, $T = 211$ K, the small step in heat capacity ($\Delta c_p \sim 0.5$ J/g K) associates with the PI and possibly amorphous PEO glass temperatures (T_g). Although the same transition is apparent in the laponite/PEO−PI nanocomposite trace with $w_{EI} = 0.5$ (with $T_g \sim 211$ K, $\Delta c_p \sim 0.25$ J/g K), exothermic/endothermic peaks due to crystallization/melting processes are absent, revealing that the PEO chains remain amorphous for certain clay concentrations. Similar results were obtained with the laponite/PEO−PI 21−5 composite. For the $w_{PEO-PI} = 0.91$ case, the PEO heat of fusion of 116 J/g results in a crystallinity of 63%. For the $w_{PEO-PI} = 0.5$ case, a weak endothermic peak is observed with a heat of fusion of only 1.4 J/g, suggesting a weak liquid crystalline order. In addition, a glass temperature is obtained at 218 K with $\Delta c_P = 0.17$ J/g K.

The corresponding diffraction patterns from the laponite/PEO−PI (21−5) clay/copolymer system at different compositions are depicted together in Figure 5, for comparison. The diffraction patterns from the w_{PEO-PI} of 0.96 and 0.91 display diffraction peaks corresponding

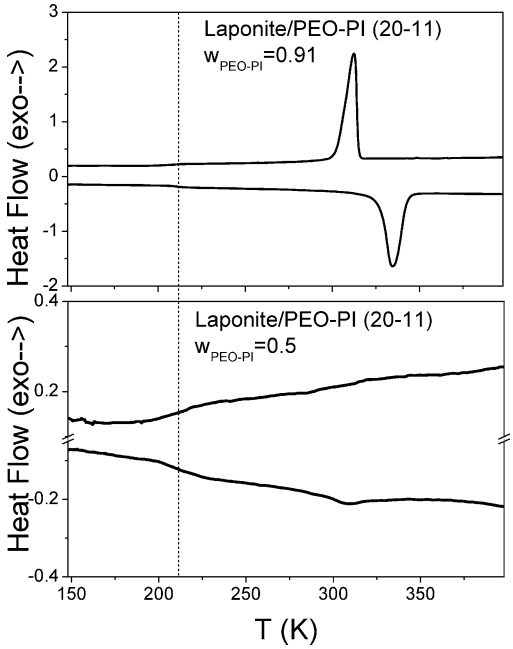

Figure 4. Differential heat flow for the laponite/PEO−PI 20−11 with a diblock weight fraction of $w_{PEO-PI} = 0.91$ (top) and the laponite/PEO−PI 20−11 nanocomposite (bottom) with a diblock weight fraction of 0.5. The data depict both the cooling curves (with a rate of 10 K/min) and the heating curves (with the same rate). Notice the suppression of PEO crystallization in the nanocomposite with the higher clay content. The vertical line at $T = 210$ K indicates the step in heat capacity at the PI and possibly PEO glass temperature.

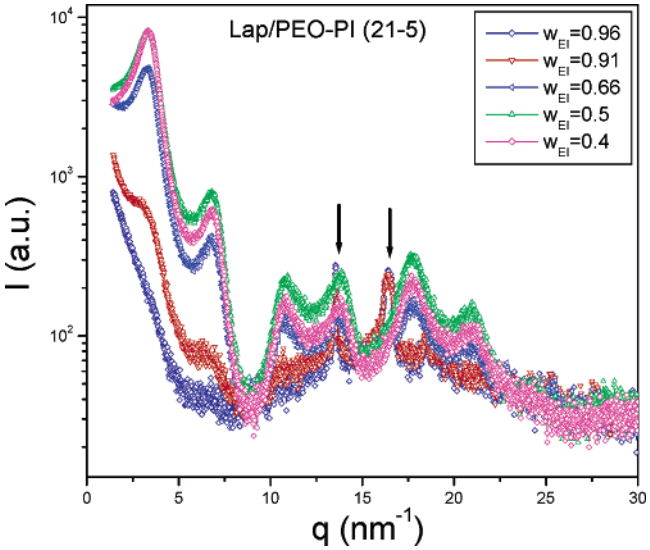

Figure 5. Wide-angle X-ray scattering patterns from the laponite/PEO−PI 21−5 nanocomposite for different copolymer compositions as indicated. Arrows give the most intense reflections of the PEO (monoclinic) unit cell.

to the PEO monoclinic unit cell as well as additional scattering due to the presence of laponite. In agreement with the DSC results, for the higher laponite concentrations the crystallization of PEO is suppressed. In addition, as with the laponite/PEO system, regular diffractions peaks are observed for the clay particles with the hydrophilic block (PEO) playing the role of springs adjusting the gallery spacing. Similar features in the diffraction patterns were obtained for the laponite/PEO−PI 20−11 system (not shown here).

(19) Alexandre, M.; Dubois, P.; Sun, T.; Garces, J. M.; Jerome, R. *Polymer* **2002**, *43*, 2123.

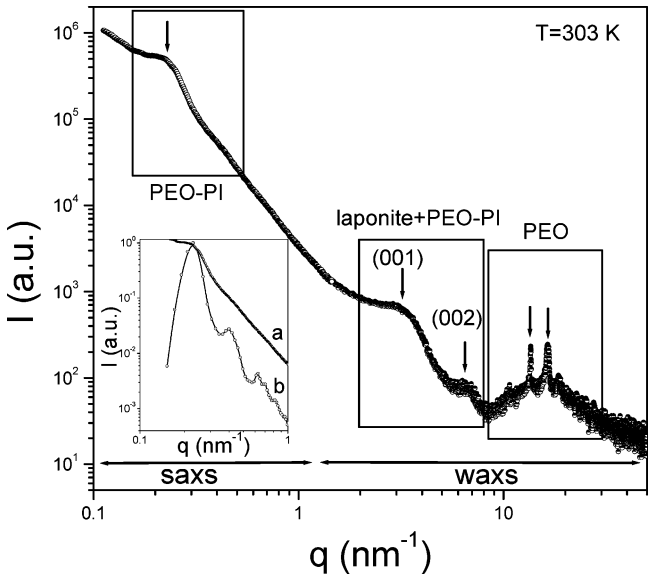

Figure 6. A composite wide- and small-angle X-ray scattering curve from the laponite/PEO−PI 21−5 nanocomposite with copolymer weight fraction of 0.91, taken at T = 303 K. Different parts of the curve are highlighted: the wide-angle part giving the sharp reflections originating from the PEO monoclinic unit cell with a unit cell parameter of 0.193 nm along the helix axis, the wide-angle part with reflections due to the composite exhibiting with laponite (001) and (002) reflections, and the small-angle range exhibiting a broad primary reflection with a spacing of 2.86 nm reflecting both the PEO crystallization and the PEO−PI nanophase separation. In the inset, the SAXS part is shown from the same laponite/PEO−PI nanocomposite at T = 353 K (curve a), i.e., above the PEO melting temperature and compared with the scattering from the pure diblock at T = 353 K (curve b). Notice the broad features in part a and the intense higher order reflections in part b due to the underlying hexagonally packed cylinders of PI.

In addition to the WAXS patterns, we have examined the possibility for longer structures originating from the contrast between the PEO and PI blocks (i.e., due to nanophase separation).[15] The phase state of the PEO−PI diblock copolymers has been examined earlier with SAXS and TEM.[16] For the PEO−PI 20−11 copolymer with f_{PEO} = 0.596, a lamellar phase is formed above 344 K; for the PEO−PI 21−5 copolymer with f_{PEO} = 0.75, hexagonally packed cylinders of PI are formed in the matrix of PEO, at T > 325 K (Table 1). Upon lowering the temperature, both equilibrium structures are destroyed and a crystalline lamellar structure is formed instead. In the SAXS region of the pattern, in both clay/copolymer composites, a strong scattering peak was found (at q^* = 0.22 nm^{-1}). A composite small- and wide-angle plot of the scattering from the laponite/PEO−PI 21−5 hybrid with w_{IE} = 0.91 is depicted in Figure 6. The figure depicts the structure over multiple length scales: first in the WAXS regime, the intense reflections are due to the PEO monoclinic unit cell of the crystalline PEO segments located outside the layer galleries; the scattering at intermediate wave vectors originates from the intercalated laponite/PEO−PI, while at even lower wave vectors the strong scattering reflects mainly the nanophase separation of the unlike blocks of the copolymer. The inset to Figure 6 compares the scattering of the pure diblock copolymer with that of the laponite/PEO−PI composite at T = 353 K, i.e., above the PEO melting temperature. The broad SAXS pattern for the composite suggests a low degree of ordering as opposed to the hexagonally packed cylinders of the amorphous PI within the amorphous PEO matrix (reflections with relative positions $1:3^{1/2}:4^{1/2}:7^{1/2}$). The inability of the block copolymer to form the same well-ordered nanostructures in the composite reflects the packing frustration of the intercalated PEO blocks, despite the similarity of the PEO block length (2.5 nm) to the platelet size (see below). On the other hand, the broad SAXS peak may also originate from long-range correlations among the clay particles. However, the identical peak position in the composite with the pure diblock copolymer implies that the measured correlations correspond to the block copolymer size and thus they are of enthalpic origin. Nevertheless, the structure in the clay/copolymer composites with high copolymer content extents over multiple length scales (PEO crystallization, PEO intercalation, and PI−PEO nanophase separation), reflecting tandem molecular interactions.

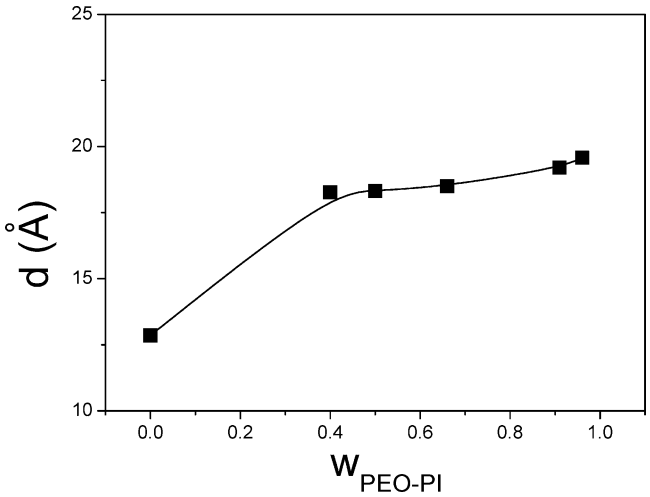

Figure 7. Dependence of the primary WAXS reflection in the laponite/PEO−PI 21−5 nanocomposites on the diblock copolymer weight fraction.

The corresponding d spacing obtained from the 001 diffraction peak in the laponite/PEO−PI composite is plotted in Figure 7 and displays similar features as with the laponite/PEO system. A PEO bilayer is formed again within the clay, and the calculated stacking height of the layers is again improved (doubled) relative to the pure laponite, as obtained from the Debye−Scherrer equation.

On the basis of the structure investigation, some very schematic structures for the laponite/PEO−PI composites are shown in Figure 8. The figure depicts (a) irregular stacking of pure clay plates, (b) the same clay plates but with a more regular spacing with intercalated PEO chains in a planar zigzag conformations and amorphous PI chains (i.e., "hairs") emanating from the plates, and (c) a down-view of the hairy plates. Elastic forces from the outer PI blocks keep the plates apart in well-defined distances. Inherent in this picture is the notion of the three levels of organization discussed earlier.

To obtain a more direct visualization of the structure suggested by the scattering experiments, we employed transmission electron microscopy from solution cast films of the composites. Before we describe the structure in the laponite/block copolymer hybrids, we comment on the size and shape of the laponite particles in

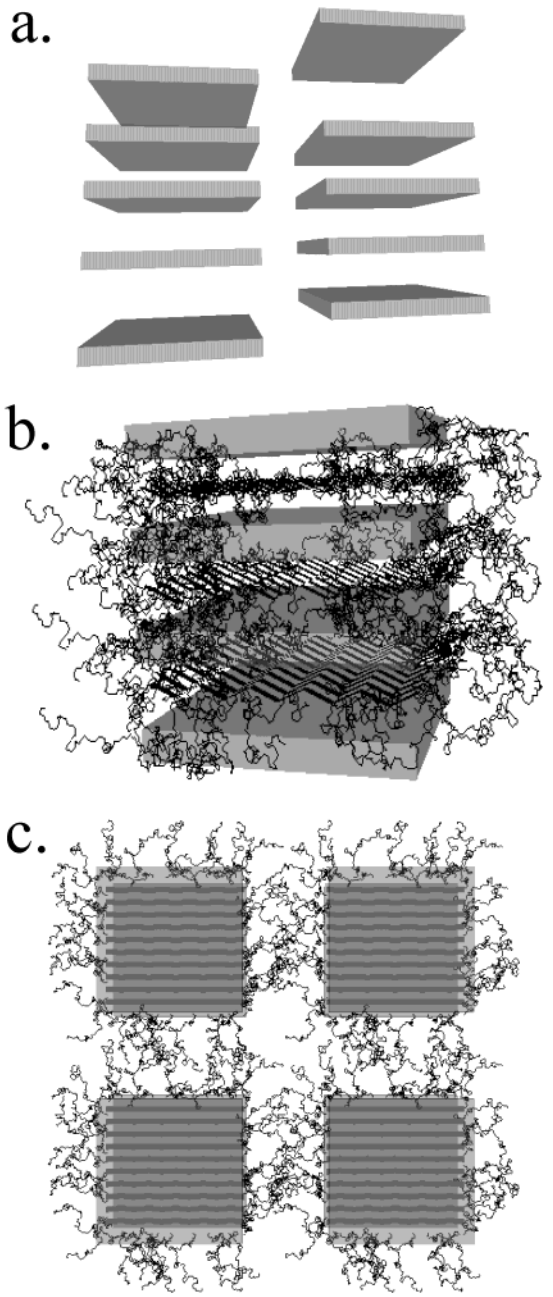

Figure 8. (a) Schematic of the pure clay plates displaying irregular spacing, (b) schematic of the structure in the laponite/PEO−PI nanocomposites depicting clay platelets filled with extended PEO chains in a planar zigzag conformation and amorphous PI chains emanating from the plates i.e., "hairy" plates, and (c) down view of the hairy plates.

aqueous solutions, a subject of intense investigation and debate.[12−14] Elementary layers of parallelepipedal shape, a network of "house of cards" where electrostatic attraction between oppositely charged faces and edges can result in flocculation, or a suspending medium of tactoids (i.e., piles of two to four superposed single platelets with a lateral dimension of about 30 nm) have been reported. Experimentally, the morphology of laponite colloids has been obtained from SAXS or small-angle neutron scattering (SANS), where the scattering intensity displays a q^{-2} dependence followed by a plateau at lower q, typical of the form factor of randomly oriented platelike colloids with a thickness of 1 nm and lateral dimensions in the range from 25 to 40 nm. On the other hand, a recent AFM investigation[12] of laponite particles deposited on mica revealed that the individual particles are not disks but rather ellipses with a height of about 1 nm and major lateral dimensions that could be described by a log-normal distribution with mean lateral dimensions of 24 ± 7 nm and 16.9 ± 5 nm.

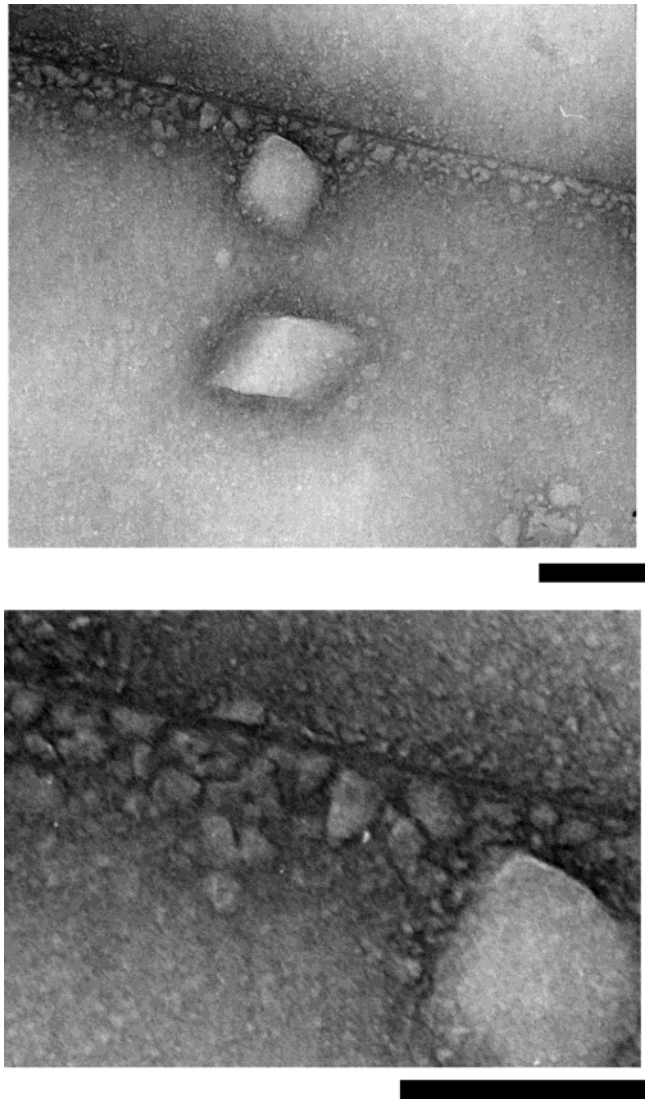

Figure 9. (top) TEM image from a stained laponite/PEO−PI nanocomposite with $w_{PEO-PI} = 0.5$. Polyisoprene appears dark due to staining. The image is taken at ambient temperature and shows laponite platelets of various sizes (from 20 to 200 nm) surrounded by darker regions (PI). (bottom) The same image shown at a larger magnification. The bar in both images corresponds to 200 nm.

To obtain a better contrast in the laponite/block copolymer system, the PI block was stained with OsO_4 and appears dark in the TEM images shown in Figure 9. The images depict clay particles surrounded by dark regions corresponding to the stained PI chains, in agreement with the schematic picture (otherwise the clay platelets would be surrounded by white regions). However, contrary to the oversimplified schematic of Figure 8, clay particles possess a variety of sizes. Some clay aggregates as large as 200 nm can be seen, but there is a majority of 10−20 nm plates. These aggregates are responsible for the absence of long-range order in the block copolymer length scale (inset to Figure 6).

Conclusion

We have investigated the structure of laponite/PEO and laponite/poly(ethylene oxide-*b*-isoprene) (PEO−PI) clay/block copolymer nanocomposites. With respect to the laponite/PEO system, we found that (i) the average stacking height is doubled relative to the pure laponite, suggesting that the elasticity provided by the PEO chains plays an important role in adjusting the layer spacing, and (ii) a PEO bilayer of chains in the planar zigzag conformation is formed for w_{PEO} up to 70%, whereas three layers are formed for higher PEO content.

With respect to the PEO−PI clay/block copolymer nanocomposites, we found that the enthalpic interactions between the unlike blocks work in tandem with the entropic interactions, favoring polymer/clay interactions, giving rise to multiple organization. More specifically we found that (i) the high laponite content (above 50%) in the composites can completely suppress the PEO crystallization and (ii) for lower laponite content there exist three levels of organization: PEO crystallization outside the layer galleries, intercalation of the hydrophilic block resulting to improved gallery spacing, and block copolymer nanophase separation of the unlike blocks with PI chains emanating from the plates and the PI elastic forces keep the plates apart.

From the broad parameter space (block composition, curvature of the block copolymer nanophase, clay size and shape, ratio of the intercalated block length to the clay size) only a small part has been explored here. Future studies will explore the structure, the mechanical properties, and the dynamics of different clay/polymer and clay/copolymer systems.

Acknowledgment. We would like to acknowledge fruitful discussions with Prof. A. Moukarika and Prof. T. Bakas as well as the use of the XRD unit of the Laboratory Network, at the UoI. We are indebted to Dr. Lieser at the MPI-P (Mainz) for the TEM study and enlightening discussions. We acknowledge G. Tsoumanis (UoI) for technical support.

CM035267M